Involvement of G$\beta\gamma$ subunits of G_i protein coupled with S1P receptor on multivesicular endosomes in F-actin formation and cargo sorting into exosomes

Received for publication, July 26, 2017, and in revised form, October 11, 2017 Published, Papers in Press, November 13, 2017, DOI 10.1074/jbc.M117.808733

Taketoshi Kajimoto[1], Nesma Nabil Ibrahim Mohamed[1], Shaymaa Mohamed Mohamed Badawy, Shubi Ambwene Matovelo, Mitsuhiro Hirase, Shunsuke Nakamura, Daisuke Yoshida, Taro Okada, Takeshi Ijuin, and Shun-ichi Nakamura[2]

From the Department of Biochemistry and Molecular Biology, Division of Biochemistry, Kobe University Graduate School of Medicine, 7-5-1 Kusunoki, Kobe 650-0017, Japan

Edited by Henrik G. Dohlman

Exosomes play a critical role in cell-to-cell communication by delivering cargo molecules to recipient cells. However, the mechanism underlying the generation of the exosomal multivesicular endosome (MVE) is one of the mysteries in the field of endosome research. Although sphingolipid metabolites such as ceramide and sphingosine 1-phosphate (S1P) are known to play important roles in MVE formation and maturation, the detailed molecular mechanisms are still unclear. Here, we show that Rho family GTPases, including Cdc42 and Rac1, are constitutively activated on exosomal MVEs and are regulated by S1P signaling as measured by fluorescence resonance energy transfer (FRET)-based conformational changes. Moreover, we detected S1P signaling-induced filamentous actin (F-actin) formation. A selective inhibitor of G$\beta\gamma$ subunits, M119, strongly inhibited both F-actin formation on MVEs and cargo sorting into exosomal intralumenal vesicles of MVEs, both of which were fully rescued by the simultaneous expression of constitutively active Cdc42 and Rac1. Our results shed light on the mechanism underlying exosomal MVE maturation and inform the understanding of the physiological relevance of continuous activation of the S1P receptor and subsequent downstream G protein signaling to G$\beta\gamma$ subunits/Rho family GTPases-regulated F-actin formation on MVEs for cargo sorting into exosomal intralumenal vesicles.

Exosomes are membrane-bound vesicles with a size of 50–100 nm that are released into the extracellular space. Exosomes contain cargoes of proteins, soluble factors, microRNAs, and mRNAs, which can be delivered to recipient cells, thereby playing a key role in intercellular communication such as antigen presentation (1), cancer progression (2), and the spreading of neurodegenerative diseases (3).

During endosomal maturation, cargo molecules are sorted into intralumenal vesicles (ILVs)[3] of multivesicular endosomes (MVEs). MVEs are then delivered to either lysosomes for degradation or plasma membranes for exosome release (4, 5). The mechanism underlying cargo sorting into ILVs destined for degradation has been clarified based on the initial discovery of yeast mutants defective in the transport to the vacuoles, the yeast analogue of mammalian lysosomes. This system utilizes the endosomal sorting complex required for transport (ESCRT) machinery responsible for sorting of mono-ubiquitinated proteins into ILVs with the aid of ESCRT machinery proteins capable of polymerization, constriction, and membrane scission (6, 7). Cargo sorting into exosomal ILVs may employ the ESCRT-independent mechanism because depletion of all four components of the ESCRT machinery only affected the population of MVEs for degradation but not for exosomal release (8). Extensive proteome studies suggest that along with cell type-specific unique cargoes, all exosomes contain a conserved set of proteins across tissues and cells, such as cytoskeletal proteins including actin and actin-binding proteins (9), although physiological roles of these cargoes remain unclear.

Sphingolipid metabolite ceramide has been proposed as a factor involved in ESCRT-independent MVE biogenesis (10). Trajkovic *et al.* (10) showed through mass spectrometric analysis that proteolipid protein 1-containing exosomes released from Oli-neu cells, a mouse oligodendroglial cell line, are enriched in ceramide, and that neutral sphingomyelinase inhibitor causes a reduction of exosome secretion. They also showed that the addition of a bacterial sphingomyelinase to giant unilamellar vesicles containing domains with differing degrees of fluidity results in inward budding formation specifically from the "raft"-like lipid phase. However, the mechanism of cargo sorting into exosomal ILVs has yet to be studied.

Ceramide is generated by hydrolysis of sphingomyelin in response to various agonists including inflammatory cytokines,

This work was supported in part by a Grant-in-Aid for challenging Exploratory Research (to S.-i. N.), a Grant-in-Aid for Scientific Research (C) (to T. O.), a Grant-in-Aid for Scientific Research (C) (to T. K.) from the Ministry of Education, Culture, Sports, Science and Technology of Japan, and a Technology Development Research Grant from the Nakatani Foundation (to T. K.). The authors declare that they have no conflicts of interest with the contents of this article.

This article contains Figs. S1–S3.

[1] Both authors contributed equally to this work.

[2] To whom correspondence should be addressed. Tel.: 81-78-382-5420; Fax: 81-78-382-5439; E-mail: snakamur@kobe-u.ac.jp.

[3] The abbreviations used are: ILVs, intralumenal vesicles; MVEs, multivesicular endosomes; ESCRT, endosomal sorting complex required for transport; S1P, sphingosine 1-phosphate; SphK, sphingosine kinase; G protein, GTP-binding protein; G_i protein, inhibitory G protein; GEFs, guanine-nucleotide exchange factors; PTX, pertussis toxin; HACPT, 2-(*p*-hydroxyanilino)-4-(*p*-chlorophenyl)thiazole; DOPE, 1,2-dioleoyl-*sn*-glycero-3-phosphoethanolamine; DiD, 1,1′-dioctadecyl-3,3,3′,3′-tetramethylindodicarbocyanine perchlorate.

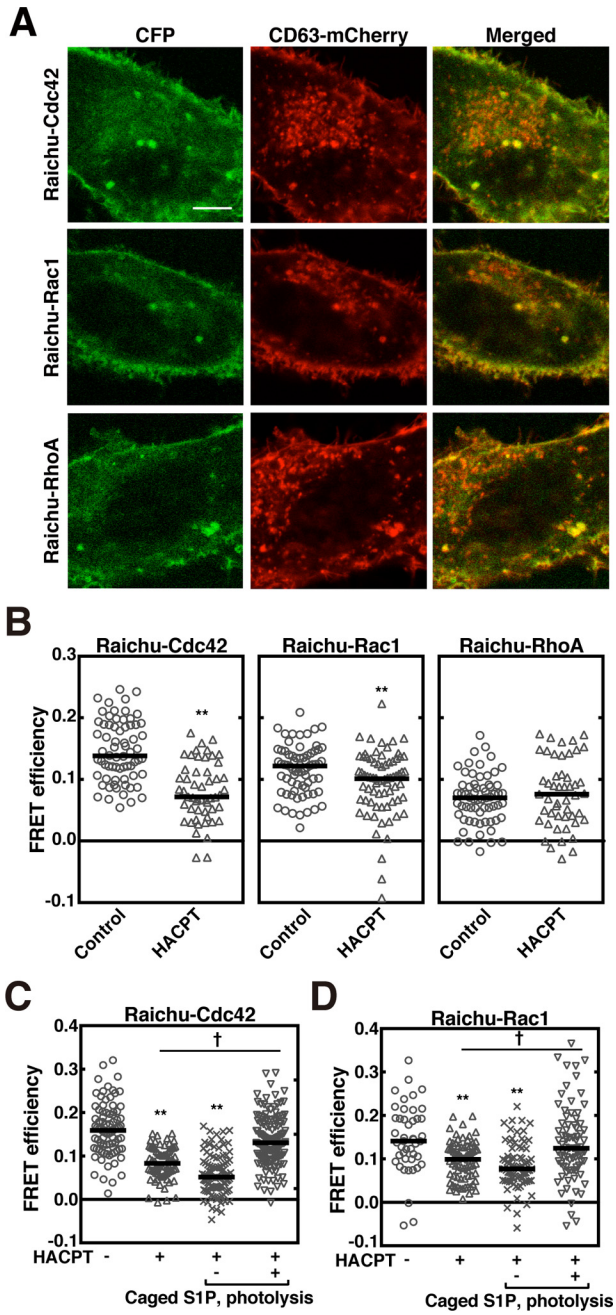

Figure 1. Continuous activation of Rho family GTPases on MVEs downstream of S1P signaling. *A,* HeLa cells expressing Raichu–Cdc42, Raichu–Rac1, or Raichu–RhoA together with both CD63–mCherry and FLAG–Rab5 (Q79L) were observed using confocal laser scanning microscope. *Scale bar*, 10 μm. *B,* HeLa cells expressing Raichu–Cdc42, Raichu–Rac1, or Raichu–RhoA together with both CD63–mCherry and FLAG–Rab5 (Q79L) were treated with or without 5 μM HACPT for 24 h, fixed, and followed by FRET analysis using confocal laser scanning microscope. The FRET efficiency was measured at CD63–mCherry-positive vesicle areas. Results are expressed as the median on scatter-dot plots ($n \geq 49$ endosomes; **, $p < 0.01$ *versus* vehicle (control); Welch's *t* test). *C,* HeLa cells expressing Raichu–Cdc42 together with both CD63–mCherry and FLAG–Rab5 (Q79L) were treated with DMSO vehicle or 5 μM HACPT for 24 h, loaded with 1 μM caged S1P, incubated for another 5 min after photolysis as indicated, and fixed. The FRET efficiency was measured at CD63–mCherry-positive vesicle areas using a confocal laser scanning microscope. Results are expressed as median on scatter-dot plots ($n \geq 72$ endosomes; **, $p < 0.01$ *versus* vehicle; †, $p < 0.05$; Welch's *t* test). *D,* HeLa cells expressing Raichu–Rac1 together with both CD63–mCherry and FLAG–Rab5 (Q79L) were treated with or without 5 μM HACPT for 24 h, loaded with 1 μM caged S1P, incubated for another 5 min after photolysis as indicated, fixed, and followed by FRET analysis as in *C*. Results are expressed as median on scatter-dot plots ($n \geq 45$ endosomes; **, $p < 0.01$ *versus* vehicle treatment; †, $p < 0.05$; Welch's *t* test).

and is implicated as an important lipid mediator for the regulation of cell cycle, differentiation, and apoptosis (11). Once ceramide is generated from sphingomyelin, it can be readily converted into a number of other bioactive sphingolipids, including sphingosine and sphingosine 1-phosphate (S1P) (12, 13). S1P, a phosphorylated product of sphingosine catalyzed by sphingosine kinase (SphK) has also been implicated as an important lipid mediator acting both inside and outside the cells (14, 15). For outside action, S1P binds to S1P receptors on the plasma membranes and regulates a variety of cell functions. All S1P receptors (type 1 to 5) are classified into a family of GTP-binding protein (G protein)-coupled receptors and show distinct expression in tissues and cells, and also unique G protein-coupling patterns suggesting distinctive functions (16).

Our recent discovery has demonstrated that sustained activation of $S1P_1$ receptor on CD63-positive MVEs in an intracrine manner is essential for cargo sorting into exosomal ILVs (17). Down-regulation of an $S1P_1$ receptor or an SphK isoform, SphK2, by specific siRNAs in HeLa cells causes reduced protein cargo contents including CD63, CD81, and flotillin 2 in exosomal ILVs of MVEs. However, an important question regarding the mechanisms underlying cargo sorting after $S1P_1$ receptor activation remains unanswered.

In the present studies, we dissected molecular events that are necessary for cargo sorting into exosomal ILVs of MVEs. We showed evidence that βγ subunits of the inhibitory G protein (G_i protein) is important in subsequent signals necessary for actin nucleation on MVEs, which is a prerequisite for cargo sorting into exosomal ILVs.

Results

Continuous activation of Rho family GTPases regulated by S1P signaling on MVEs

It has previously been shown in our laboratory that $S1P_1$ receptor-G_i signaling is continuously activated on exosomal MVEs, which serves a function in cargo sorting into exosomal ILVs of MVEs (17). During MVE maturation in ESCRT-dependent processes, several proteins with activities of polymerization and contraction are involved in inward budding and ILV formation (7). We reasoned therefore that some proteins capable of polymerization/depolymerization, including the actin cytoskeleton, might be important in ESCRT-independent cargo sorting into exosomal ILVs on MVEs. In this context we tested whether the activity of Rho family GTPases such as Cdc42, Rac1, and RhoA is under control of S1P signaling on MVEs. First, the activity of each GTPase was measured by fluorescence resonance energy transfer (FRET)-based conformational changes. These FRET probes have been verified in their cellular localization as compared with that of their native counterparts (18). When these one-molecular FRET probes, Raichu–Cdc42, Raichu–Rac1, and Raichu–RhoA were expressed in HeLa cells, all the probes showed the expression in both plasma membranes and CD63-positive MVEs (Fig. 1*A*). Then, the FRET values in the CD63-positive MVEs were analyzed

using a acceptor photobleaching method in the fixed cells. The FRET efficiency using a Raichu–Cdc42 probe on CD63-positive MVEs was high (Fig. 1*B*, Raichu–Cdc42 and see supplemental Fig. S1*A*), which was decreased by an SphK inhibitor, 2-(*p*-hydroxyanilino)-4-(*p*-chlorophenyl)thiazole (HACPT). This suggests that Cdc42 on MVEs is constantly activated by S1P signaling, which is reminiscent of a sustained activation of the $S1P_1$ receptor on MVEs (17). Similarly, Rac1 was continuously activated under regulation of the S1P signal on MVEs (Fig. 1*B*, Raichu–Rac1, and see Fig. S1*A*), however, the activity of RhoA on MVEs was low under basal conditions and was insensitive to HACPT (Fig. 1*B*, Raichu–RhoA and see Fig. S1*A*). To further strengthen the importance of the S1P signal on the regulation of these GTPase activities on MVEs, rescue experiments using a caged S1P were conducted. After loading caged S1P, the effect of HACPT on each GTPase activity in cells expressing either Raichu–Cdc42 or Raichu–Rac1 was measured before and after photolysis to release S1P. In both GTPases, the inhibition caused by HACPT was almost completely rescued by photolysis-activated caged S1P (Fig. 1, *C* and *D,* and see Fig. S1, *B* and *C*), confirming the importance of the S1P signal in the activation of both Cdc42 and Rac1 on MVEs.

Involvement of β and γ subunits of the G protein (Gβγ subunits) of G_i downstream of $S1P_1$ receptor in the activation of Rho family GTPases on MVEs

To identify the downstream signal after S1P receptor activation leading to regulating the Cdc42 and Rac1 activity, the effects of G_i subunit-specific inhibitors on the regulation of the Rho family GTPases on MVEs were studied. M119 is an inhibitor screened for the ability to compete for binding to the "hot spot" of Gβγ subunits, and was shown to inhibit the Gβγ subunits-related phenomena, such as agonist-induced activation of phospholipase Cβ and PI3 kinase (19). In HeLa cells expressing an exosomal cargo marker CD63 and Raichu–Cdc42, Cdc42 activity on CD63-positive MVEs was strongly inhibited by M119 to an extent similar to the treatment with pertussis toxin (PTX), which is known to make G_i-coupled receptors uncoupled from G_i to the agonist stimulation (20). However, the activity was unaltered by the $G\alpha_i$ subunit inhibitor (NF023) as judged by FRET-based conformational changes (Fig. 2*A* and see Fig. S2*A*). On the other hand, Rac1 activation on MVEs was suppressed by M119 and NF023 (Fig. 2*B* and see Fig. S2*B*).

To show a causal relationship between Gβγ subunit regulation of the Rho family GTPases on MVEs and cargo sorting into exosomal ILVs, the effect of G_i subunit-specific inhibitors on the amount of CD63 sorted in ILVs was studied. M119 or PTX treatment of cells expressing CD63 showed a clear suppression of CD63 content in the lumen of MVEs as compared with vehicle treatment (Fig. 3*A*, *arrows*). Quantitative data of cargo sorting into ILVs as measured by the criterion (Fig. 3*B*) showed that M119 strongly reduced the cargo content in MVEs to an extent similar to that obtained with PTX treatment, whereas NF023 showed milder effects (Fig. 3*C*). M119 inhibited the CD63 sorting in a dose-dependent manner with a half-maximal inhibition at 0.3 μM and reaching a maximum at 10 μM (Fig. 3*D*). These results suggest that the Gβγ subunits play a principal role in the

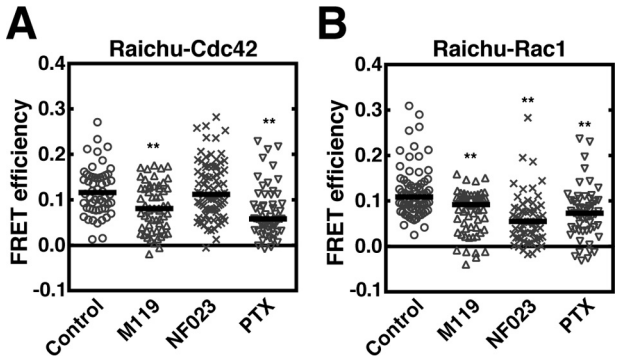

Figure 2. Regulation of Rho family GTPases on MVEs by Gβγ subunits. *A,* HeLa cells expressing Raichu–Cdc42 together with CD63–mCherry and FLAG–Rab5 (Q79L) were treated with or without 10 μM M119, 10 μM NF023, or 100 ng/ml of PTX for 24 h, fixed, and followed by FRET analysis using a confocal laser scanning microscope. The FRET efficiency was measured at CD63–mCherry-positive vesicle areas. Results are expressed as median on scatter-dot plots ($n \geq 54$ endosomes; **, $p < 0.01$ *versus* vehicle (control); Welch's *t* test). *B,* HeLa cells expressing Raichu–Rac1 together with CD63–mCherry and FLAG–Rab5 (Q79L) were treated with or without 10 μM M119, 10 μM NF023, or 100 ng/ml of PTX for 24 h, fixed, and followed by FRET analysis as in *A*. Results are expressed as the median on scatter-dot plots ($n \geq 55$ endosomes; **, $p <$ 0.01 *versus* vehicle (control); Welch's *t* test).

regulation of cargo sorting into exosomal MVEs. The involvement of Gβγ subunits in this phenomenon was further strengthened by the subunit-specific "scavenger experiment" (21), where expression of the carboxyl terminus of G protein-coupled receptor kinase 2-derived peptide (GRK2ct) was expected to cause sequestration of the endogenous Gβγ subunits on MVEs and inhibit their function. Remarkably, the expression of GRK2ct resulted in a significant reduction of CD63 sorting (Fig. 3*E*), confirming the involvement of the Gβγ subunits in this phenomenon.

Involvement of Gβγ subunits-dependent guanine-nucleotide exchange factors (GEFs) for Rho family GTPases in the regulation of Cdc42 and Rac1 on MVEs

It has recently been shown that the Gβγ subunits dissociated from G_i proteins interact directly with and activate P-Rex1, a Rac-specific GEF (22) and PLEKHG2, a GEF for both Rac and Cdc42 (23). To see if these GEFs are involved in the activation of Cdc42 and Rac1 on MVEs, the effect of knockdown of these GEFs using a gene-silencing technique on the GTPase activity of Cdc42 and Rac1 on MVEs was next addressed. Compared with control siRNA, treatment of cells with PLEKHG2–siRNA or P-Rex1–siRNA resulted in the reduction of the amount of mRNAs for the respective proteins (see Fig. S3, *A* and *B*), showing the validity of the experiment. When cells were treated with PLEKHG2–siRNA, both Cdc42 and Rac1 activity on MVEs were significantly inhibited (Fig. 4, *A* and *B*). On the other hand, knockdown of P-Rex1 resulted in only inhibition of Rac1 activity on MVEs (Fig. 4, *A* and *B*) as reported previously (22). These results strongly suggest that either or both of these GEFs are downstream signaling molecules leading to Cdc42 and Rac1 activation through the Gβγ subunits on MVEs. In fact, knockdown of either GEF resulted in the suppression of CD63 sorting (Fig. 4*C*), which demonstrates the involvement of these GEFs in cargo sorting into MVEs.

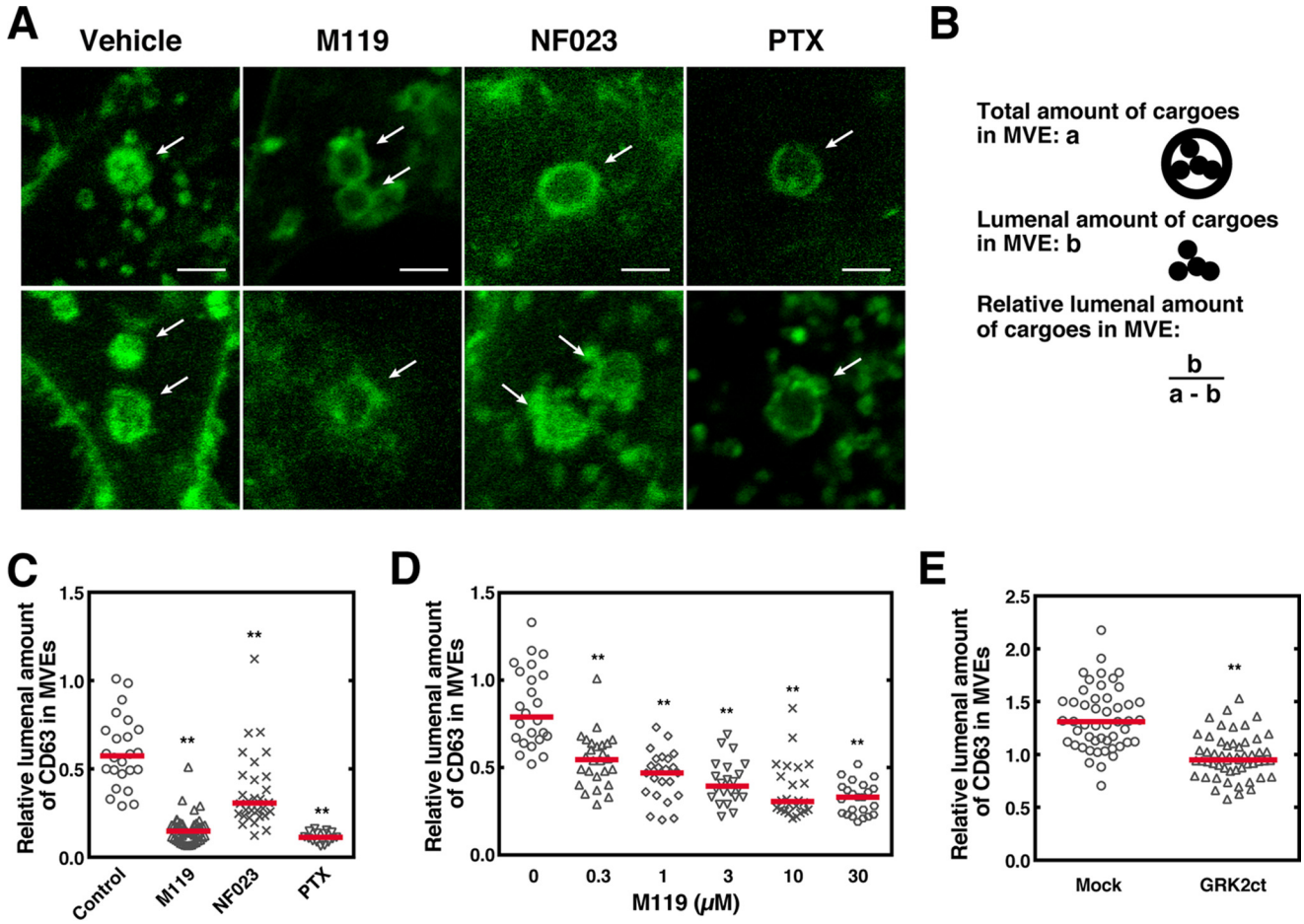

Figure 3. Involvement of Gβγ subunits of PTX-sensitive G proteins in CD63 sorting into ILVs of MVEs. *A,* HeLa cells expressing both CD63–GFP and Rab5 (Q79L)–DsRed were treated with or without 10 μM M119, 10 μM NF023, or 100 ng/ml of PTX for 24 h, fixed, and observed using a confocal laser scanning microscope. *Scale bar*, 10 μm. Representative data from 3 independent experiments are shown. *B,* schematic representation of MVE cargo sorting analysis. *C,* HeLa cells expressing both CD63–GFP and Rab5 (Q79L)–DsRed were treated with M119, NF023, or PTX as in *A* and was followed by MVE cargo sorting analysis. Results are expressed as the median on scatter-dot plots ($n \geq 24$ endosomes; **, $p < 0.01$ *versus* vehicle (*Control*); Welch's *t* test). *D,* HeLa cells expressing both CD63–GFP and Rab5 (Q79L)–DsRed were treated with various concentrations of M119 as specified followed by MVE cargo sorting analysis. Results are expressed as the median on scatter-dot plots ($n \geq 20$ endosomes; **, $p < 0.01$ *versus* vehicle (0 μM); Welch's *t* test). *E,* HeLa cells expressing both CD63–GFP and Rab5 (Q79L)–DsRed together with mock or FLAG-GRK2ct were analyzed for MVE cargo sorting. Results are expressed as the median on scatter-dot plots ($n \geq 50$ endosomes; **, $p < 0.01$ *versus* vehicle (control); Welch's *t* test).

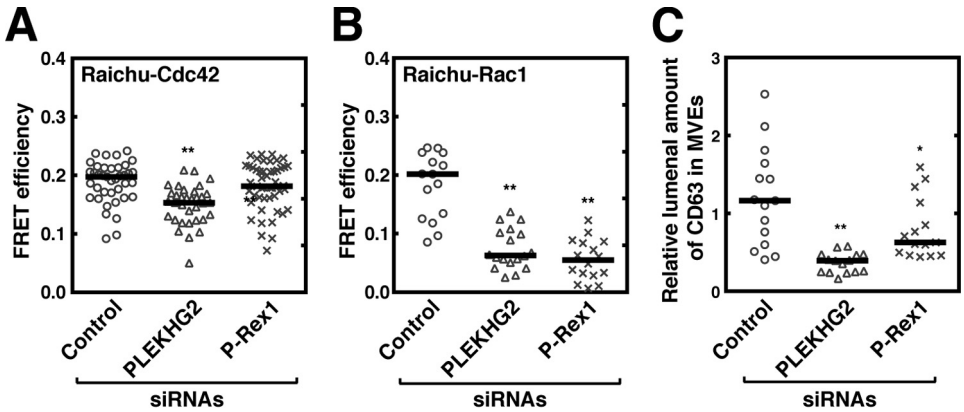

Figure 4. Involvement of Gβγ subunit-dependent GEFs for Rho family GTPases in the regulation of Cdc42 and Rac1 on MVEs. HeLa cells cotransfected with control, PLEKHG2–, or P-Rex1–siRNA together with vectors encoding both CD63–mCherry and FLAG–Rab5 (Q79L) and either Raichu–Cdc42 (*A*) or Raichu–Rac1 (*B*) were fixed and followed by FRET analysis using confocal laser scanning microscope. The FRET efficiency was measured at CD63–mCherry-positive vesicle areas. Results are expressed as median on scatter-dot plots ($n \geq 37$ endosomes; **, $p < 0.01$ *versus* control siRNA (control); Welch's *t* test). *C,* HeLa cells transfected with a vector encoding both CD63–GFP and Rab5 (Q79L)–DsRed together with control, PLEKHG2-, or P-Rex1–siRNA were cultured for 72 h. Cells were fixed, followed by MVE cargo sorting analysis. Results are expressed as the median on scatter-dot plots ($n \geq 15$ endosomes; **, $p < 0.01$; *, $p < 0.05$ *versus* vehicle (control); Welch's *t* test).

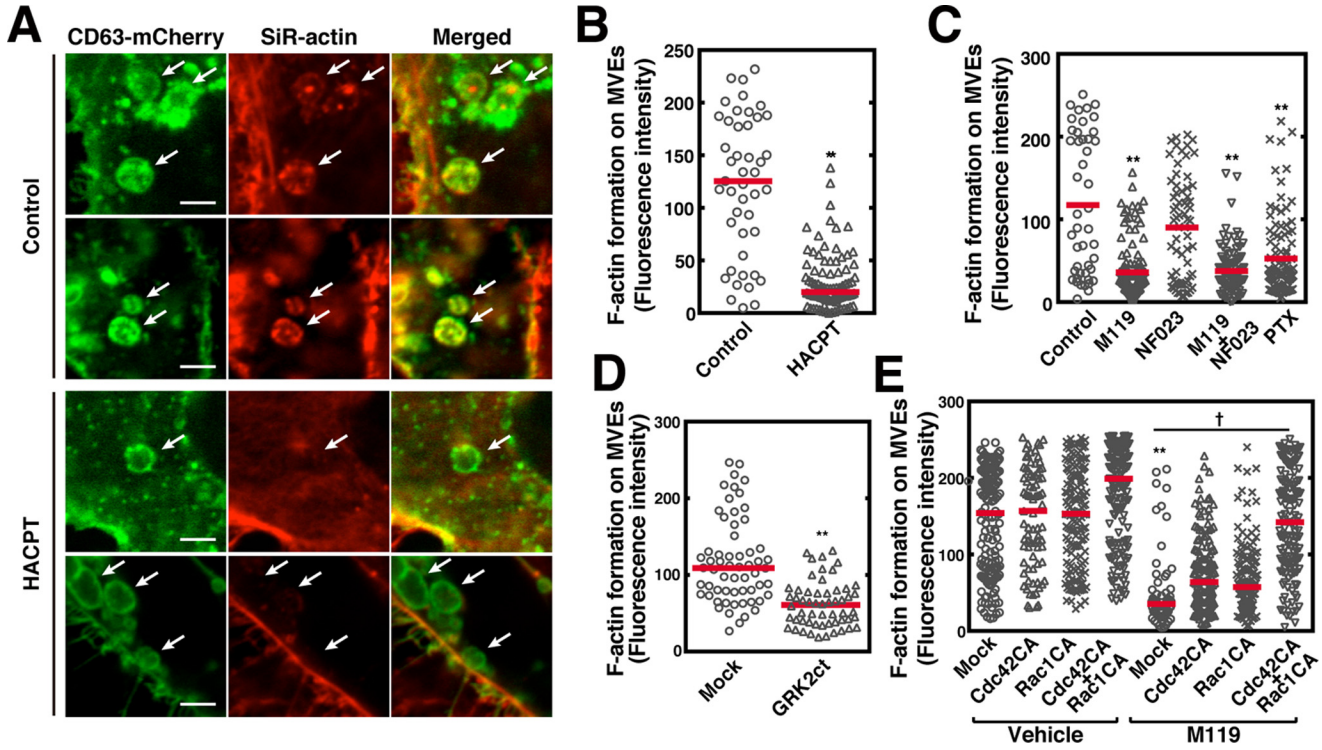

Figure 5. Essential role of Gβγ subunits of G_i signaling in actin nucleation on MVEs. *A,* HeLa cells expressing both CD63–mCherry and FLAG–Rab5 (Q79L) were loaded with SiR–actin with or without 5 μM HACPT for 24 h, fixed, and followed by observing the mCherry and SiR fluorescence using a confocal laser scanning microscope. *White arrows* indicate CD63–mCherry-positive MVEs. *Scale bar*, 5 μm. *B,* fluorescence intensity of the filamentous SiR-actin at CD63–mCherry-positive MVE areas as in *A* was quantitated. Results are expressed as median on scatter-dot plots ($n \geq 45$ endosomes; **, $p < 0.01$ *versus* vehicle (control); Welch's *t* test). *C,* HeLa cells expressing both CD63–mCherry and FLAG–Rab5 (Q79L) were loaded with SiR–actin with or without 10 μM M119, 10 μM NF023, or 100 ng/ml of PTX for 24 h, fixed, followed by F-actin formation analysis as in *A* using a confocal laser scanning microscope. The fluorescence intensity of SiR–actin at CD63–mCherry-positive MVE areas was quantitated. Results are expressed as the median on scatter-dot plots ($n \geq 45$ endosomes; **, $p < 0.01$ *versus* vehicle (control); Welch's *t* test). *D,* HeLa cells expressing both CD63–mCherry and FLAG–Rab5 (Q79L) together with mock or FLAG-GRK2ct were loaded with SiR–actin for 24 h and analyzed for F-actin formation as in *A*. Results are expressed as median on scatter-dot plots ($n \geq 50$ endosomes; **, $p < 0.01$ *versus* vehicle (control); Welch's *t* test). *E,* HeLa cells transfected with mock, Myc–Cdc42 (Q61L), or Myc–Rac1 (Q61L) together with both CD63–mCherry and FLAG–Rab5 were loaded with SiR–actin with or without 10 μM M119 for 24 h, fixed, and followed by F-actin formation analysis as in *A* using a confocal laser scanning microscope. The fluorescence intensity of SiR–actin at CD63–mCherry-positive MVE areas was quantitated. Results are expressed as median on scatter-dot plots ($n \geq 71$ endosomes; *, $p < 0.05$; **, $p < 0.01$ *versus* mock of vehicle control; †, $p < 0.05$; Welch's *t* test).

Essential role of Gβγ subunits-regulated actin nucleation on MVEs in cargo sorting into exosomal ILVs

An important issue to be addressed is whether actin nucleation on MVEs actually has a role in cargo sorting into exosomal ILVs. First, actin nucleation on MVEs was monitored by SiR-actin fluorescence, which is a cell-permeable reagent and binds specifically and reversibly to filamentous actin (F-actin) but poorly to globular actin. Under control conditions exosomal MVEs contained CD63 both in limiting membranes and within ILVs, whereas HACPT treatment resulted in a decrease in CD63 in ILVs, suggesting the inhibition of cargo sorting by this inhibitor (Fig. 5*A*) is consistent with the previous report (17). Importantly, F-actin formation was also observed in CD63-positive MVEs under control conditions (Fig. 5*A*). Notably, HACPT treatment resulted in a robust inhibition of F-actin formation on MVEs (Fig. 5, *A* and *B*), suggesting regulation of F-actin formation by S1P signaling on MVEs. Next, the effects of G_i protein subunit inhibitors on actin nucleation on MVEs were tested. Importantly, actin nucleation was strongly inhibited by M119 consistent with the involvement of G_i as suggested by PTX sensitivity (Fig. 5*C*). NF023 was less effective in inhibiting F-actin formation. To confirm whether the Gβγ subunits indeed regulate the F-actin formation on MVEs, the effect of sequestration of endogenous Gβγ subunits by the expression of a "scavenger" was carried out next. The expression of GRK2ct significantly suppressed the F-actin formation on MVEs (Fig. 5*D*), validating the role of the subunits in these phenomena. To substantiate the idea that F-actin formation on MVEs is a downstream event regulated by the Gβγ subunits, we then conducted rescue experiments using constitutively active Cdc42 or Rac1 in inhibition caused by M119 of F-actin formation. Inhibition of F-actin formation caused by M119 was partially reversed by either constitutively active Q61L–Cdc42 (Cdc42CA) or Q61L–Rac1 (Rac1CA), respectively (Fig. 5*E*). Simultaneous expression of both Cdc42CA and Rac1CA almost completely rescued the M119-induced inhibition of actin polymerization. These results strongly suggest that Cdc42 and Rac1 are downstream targets of the Gβγ subunits and that activation of both of these GTPases is required for actin nucleation on MVEs. Finally, causal relationship between F-actin formation on MVEs and cargo sorting into exosomal ILVs were addressed. Treatment of HeLa cells expressing CD63–mCherry with M119 resulted in the inhibition of the cargo content in ILVs as compared with vehicle treatment (Fig. 6). Expression of either Cdc42CA or Rac1CA had little effect on the inhibition caused by M119. However, simultaneous expression of both GTPases

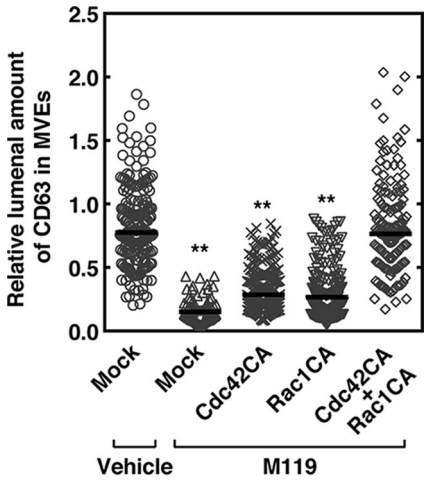

Figure 6. Important role of Gβγ subunit-regulated F-actin formation on MVEs in cargo sorting into exosomal ILVs. HeLa cells expressing both CD63–mCherry and FLAG–Rab5 (Q79L) together with mock, Myc–Cdc42 (Q61L) (Cdc42CA), and/or Myc-Rac1 (Q61L) (Rac1CA) as specified were treated without (vehicle) or with 10 μM M119 for 24 h, fixed, and fluorescence intensity of the CD63-mCherry sorted in the endosomal lumen of MVEs was measured using a confocal laser scanning microscope. Results are expressed as the median on scatter-dot plots ($n \geq 50$ endosomes; **, $p < 0.01$ *versus* mock of vehicle control; Welch's *t* test).

completely rescued the M119 inhibition, suggesting full F-actin formation on MVEs are required for cargo sorting into exosomal ILVs.

Inhibition of F-actin formation by the pharmacological inhibitor cytochalasin B resulted in decreased lumenal content of CD63 in MVEs and released exosomes leaving the number of exosomes unchanged

We manipulated the actin polymerization by cytochalasin B, a fungal metabolite, that binds to F-actin filaments and prevents its polymerization, and analyzed the effect on cargo sorting into exosomal ILVs of MVEs and on cargo contents in purified exosomes. As expected, cytochalasin B strongly inhibited the lumenal content of CD63–mCherry in MVEs compared with the vehicle control (Fig. 7*A*). Similarly, cytochalasin B strongly inhibited the cargo (CD63) content in exosomes compared with a control vehicle (Fig. 7*B*) as measured by a single exosome assay, which has recently been developed in our laboratory (17). Note that although cytochalasin B treatment strongly inhibited the cargo content in exosomes, total exosome numbers remained almost unchanged (Fig. 7*B*, compare N number 460 (control) *versus* 501 (cytochalasin B)). This implies that ILV biogenesis itself has no connection with actin polymerization.

Discussion

It has been well known that the active form of Cdc42 and Rac1 interacts with N-WASP (24, 25) and WAVE complexes (26, 27), respectively, resulting in activation of the actin-related protein 2/3 complex (Arp2/3), a protein complex essential for the nucleation of actin polymerization and the formation of F-actin networks (28). Compared with recognized roles for actin rearrangements in the plasma membrane, relatively little is known about how actin nucleation influences late endosome maturation. In the present studies we have demonstrated that the Gβγ subunits derived from G_i subunit dissociation after S1P receptor activation on MVEs are important in subsequent activation of the Rho family GTPases, Cdc42 and Rac1 on MVEs. Although P-Rex1 has been shown to interact with $S1P_1$ receptor at the cell surface to facilitate cell migration in response to S1P (29), the physiological role of F-actin formation on MVEs was unclear. We have shown that knockdown of the Gβγ subunit-dependent GEFs such as P-Rex1 and PLEKHG2 by siRNA resulted in reduced activity of Cdc42 and Rac1 on MVEs in HeLa cells (Fig. 4). This result indicates that F-actin formation on MVEs is constantly regulated by the Gβγ subunits through these GEFs in HeLa cells. This observation matches well with our previous observation that the $S1P_1$ receptor is continuously activated on MVEs and transmitting the G_i protein signal at the receptor (17).

We have also demonstrated the importance of F-actin formation on MVEs in the cargo sorting into exosomal vesicles of MVEs as suggested by findings that the Gβγ subunits-selective inhibitor, M119, induced inhibition of both Cdc42 and Rac1 activity (Fig. 2) resulting in inhibition of both F-actin formation on MVEs (Fig. 5*C*) and CD63 sorting into ILVs of MVEs (Figs. 3 and 6). Furthermore, the M119-induced inhibition of GTPase activity of Cdc42 and Rac1 and cargo sorting into exosomal ILVs was completely rescued by the simultaneous expression of constitutively active Cdc42CA and Rac1CA (Figs. 5*D* and 6, respectively).

We have previously reported that transiently expressed green fluorescent protein (GFP)-tagged SphK2 (SphK2–GFP), but not SphK1–GFP, showed a good colocalization with CD63-positive late endosomes, and that endogenous SphK2 and CD63 were well colocalized (17). Generation of S1P catalyzed by SphK2 may be responsible for continuous activation of S1P receptors on MVEs. The mechanism underlying the targeting of SphK2 to MVEs and topological movement of S1P from the cytoplasmic surface to lumen of MVEs for the activation of the receptor or through other mechanisms, *e.g.* generation of S1P in the lumenal surface of MVEs, needs to be clarified.

In conclusion, we have demonstrated that continuous activation of PTX-sensitive S1P receptors such as $S1P_1$ receptor on MVEs keeps transmitting signals into exosomal MVEs. The dissociated Gβγ subunits from the Gα subunit interact with the relevant GEFs, PLEKHG2 and P-Rex1, leading to Cdc42 and Rac1 activation, which are necessary for actin nucleation on MVEs. F-actin formation presumably provides rails for cargoes during sorting into exosomal ILVs (Fig. 8).

Experimental procedures

Reagents

PTX was purchased from Wako Pure Chemical Industries (Osaka, Japan). Gβγ modulator I (M119) and HACPT were obtained from Calbiochem. NF023 was purchased from Sigma. Caged S1P was purchased from Santa Cruz Biotechnology (Dallas, TX). All other materials were reagent grade.

Plasmids and mutations

Human CD63 was amplified and cloned into pEGFP-N1 or pmCherry-N1 (Clontech Laboratories, Mountain View, CA) for making GFP- or mCherry-tagged CD63, respectively.

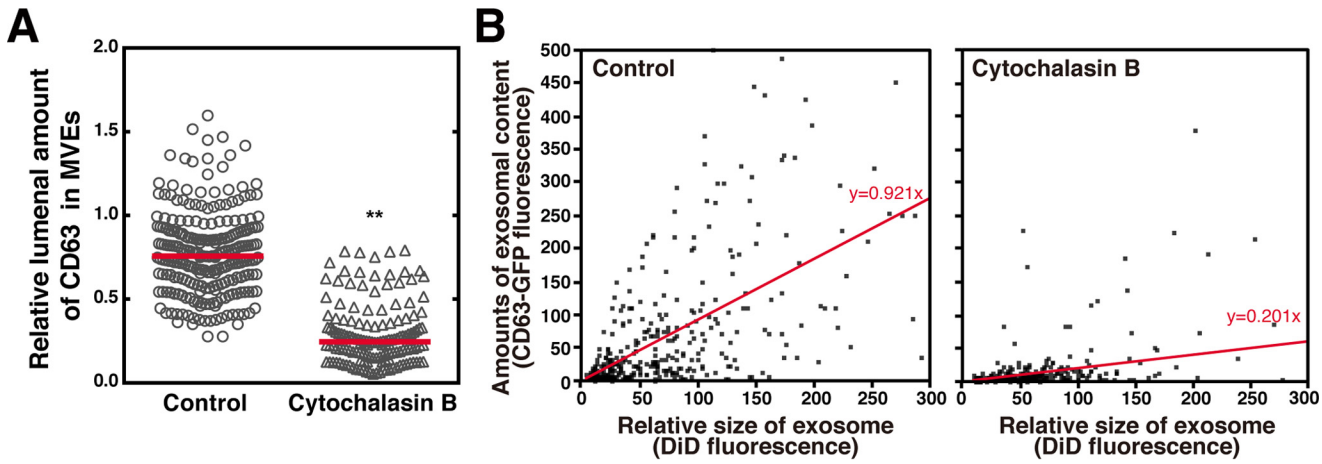

Figure 7. Inhibition of F-actin formation by cytochalasin B results in reduced cargo content in both MVEs and exosomes, leaving the total exosome number unchanged. *A,* HeLa cells expressing both CD63–GFP and Rab5 (Q79L)–DsRed were treated with or without 10 μM cytochalasin B, fixed, followed by MVE cargo sorting analysis. Results are expressed as the median on scatter-dot plots ($n \geq 162$ endosomes; **, $p < 0.01$ *versus* vehicle (control); Welch's *t* test). *B,* HeLa cells expressing CD63–GFP were treated with or without 10 μM cytochalasin B for 24 h, followed by exosomal cargo density analysis. Exosomes prepared by a sequential centrifugation from the cell culture media (5×10^5 cells) were resuspended in an equivolume buffer, labeled with DiD, and immobilized on a streptavidin functionalized glass surface (see "Experimental procedures"). Images of the CD63–GFP and DiD fluorescence were acquired with a confocal laser scanning microscope. The fluorescence intensity of DiD and CD63–GFP in DiD-labeled exosomes obtained from the images were plotted on the correlation diagram for each exosome. Note that the number of exosomes in the control and cytochalasin B treatments were 460 and 501, respectively, indicating that cytochalasin B treatment has little or no effect on the total number of exosomes.

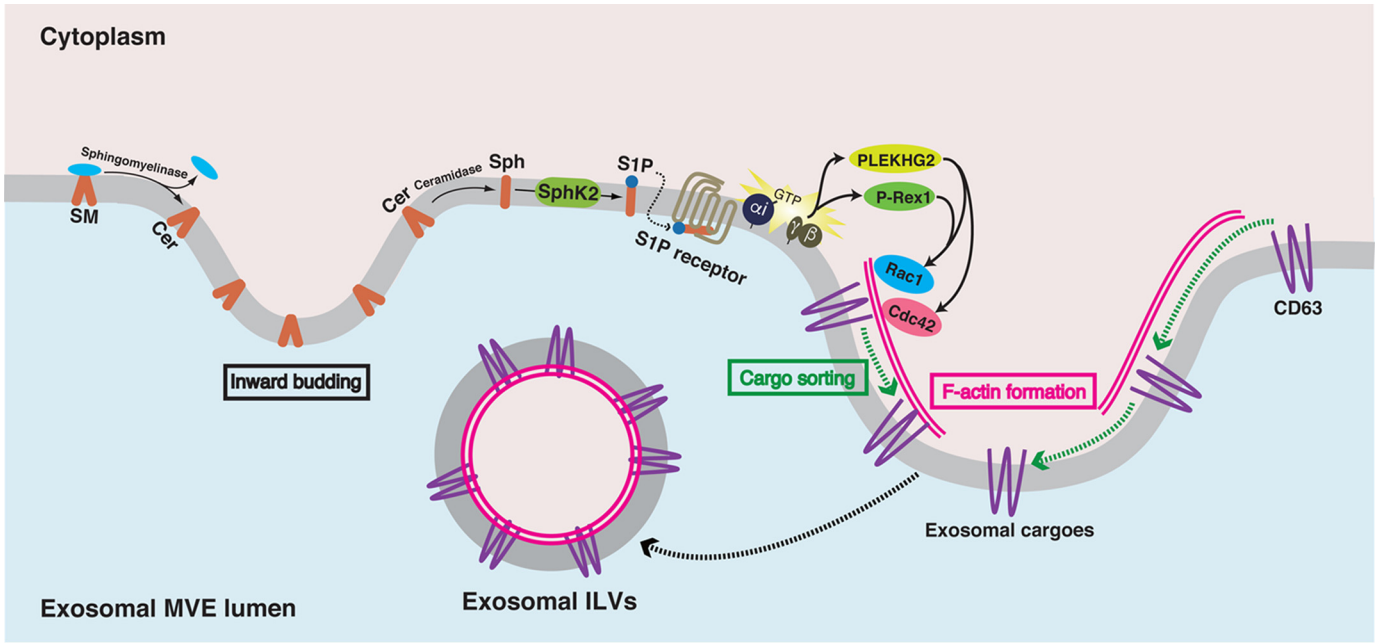

Figure 8. Current model for cargo sorting into exosomal ILVs after S1P receptor activation on MVEs. During MVE maturation sphingomyelin is hydrolyzed by sphingomyelinase to produce ceramide (*Cer*) and phosphorylcholine. Ceramide is known to induce inward budding at the MVE membrane to produce ILVs (10). Once ceramide is generated it is readily hydrolyzed to sphingosine (*Sph*) catalyzed by ceramidase. SphK2 phosphorylates Sph to form S1P, which is pivotal in exosomal cargo sorting into ILVs. Continuous activation of the $S1P_1$ receptor on MVEs keeps transmitting signals for the maturation of exosomal MVEs (17). As a result of the continuous receptor activation, the Gβγ subunits dissociated from G_i interact with PLEKHG2 and P-Rex1, which in turn cause activation of both Cdc42 and Rac1, which is prerequisite for actin nucleation on MVEs. F-actin formation on MVEs is necessary for cargo sorting into exosomal ILVs presumably providing rails for cargoes.

Human Rab5 was amplified and cloned into FLAG–pCMV5 for making N terminally FLAG-tagged Rab5. For FLAG–Rab5 (Q79L), glutamine 79 was mutated to a leucine using a QuikChange site-directed mutagenesis protocol. DsRed-tagged Rab5 (Q79L) was generated by subcloning the Rab5 (Q79L) into pDsRed-monomer-C1 (Clontech). pRaichu–Cdc42, pRaichu–Rac1, and pRaichu–RhoA were kindly provided from Dr. M. Matsuda (Kyoto University). Myc-Cdc42 (Q61L) (plasmid number 12974) and Myc-Rac1 (Q61L) (plasmid number 12983) were purchased from Addgene (Cambridge, MA). The C-terminal (amino acids 495–689) of human GRK2 (GRK2ct) (21) was amplified and cloned into FLAG-pCMV5 for making N terminally FLAG-tagged GRK2ct.

Cell cultures and transfections

HeLa cells purchased from Riken Cell Bank (Tsukuba, Ibaraki, Japan) were maintained in Dulbecco's modified Eagle's medium (Wako Pure Chemical Industries, Osaka, Japan) con-

taining 10% fetal bovine serum and 1% penicillin/streptomycin at 37 °C in 5% CO_2. Cells were plated onto glass-bottomed 35-mm culture dishes (MatTek, Ashland, MA) or 60-mm culture dishes (Corning, NY) prior to transfection. Transient transfection was carried out using FuGENE HD (Promega) or Lipofectamine 2000 (Invitrogen Corp.) for HeLa cells. All experiments were performed 2 to 3 days after transfection.

Real-time quantitative reverse transcription-PCR

Total RNA was extracted from HeLa cells (2×10^6 cells) using NucleoSpin RNA II (Macherey-Nagel) according to the manufacturer's instructions. 1 μg of RNA was used for reverse transcription (ReverTra Ace qPCR RT kit, TOYOBO). Quantitative PCR was performed with SYBR Premix (Takara) on ABI Prism 7000. The expression level of glyceraldehyde-3-phosphate dehydrogenase (GAPDH) was used as the internal control. The primer sequences (sense and antisense) were ask follows: for human PLEKHG2, 5′-TTCACTGTCTCCAGCGCCTC-3′ and 5′-TTTTGGGGGCACAATGCAGG-3′; for human P-Rex1, 5′-TGGGCACCGAGAGGGACTAC-3′ and 5′-TGAGGCCCTTCTCCACTGAG-3′; for human GAPDH, 5′-GCCATCAATGACCCCTTCATT-3′ and 5′-TCTCGCTCCTGGAAGATGG-3′.

Loading of caged S1P

HeLa cells grown on glass-bottomed culture dishes were preloaded with 1 μM caged S1P for 30 min. After washing out the media, dishes were then flashed with UV light (254 nm) for 20 s for photolysis of caged S1P. Then cells were incubated in culture conditions for the indicated time.

FRET analysis

HeLa cells were transiently cotransfected with pRaichu–Cdc42, pRaichu–Rac1, or pRaichu–RhoA, and CD63–mCherry and FLAG–Rab5 (Q79L) at a ratio of 2:1:8 using FuGENE HD (Promega). In some experiments HeLa cells were cotransfected with plasmid DNAs described above and control siRNA, P-Rex1 siRNA (5′-AAUUUUAAGAAAACAUUCCdCdA-3′ and 5′-GGAAUGUUUUCUUAAAAUUdCdA-3′) or PLEKHG2 siRNA (5′-UUAACAAAACAUUAAUGACdAdT-3′ and 5′-GUCAUUAAUGUUUUGUUAAdTdA-3′) using Lipofectamine 2000. To minimize off-target effects, these siRNAs were designed by using siDirect 2.0 Web server (30) and transfected into cells at low (5 nM) concentrations. Three days after cotransfection, cells were treated with the indicated reagents followed by fixed with 4% paraformaldehyde in phosphate-buffered saline. The CD63–mCherry-positive vesicle of interest was subjected to FRET analysis with the acceptor photobleaching method using a LSM 510 META (Carl Zeiss, Oberkochen, Germany) with a ×63 oil plan-apochromat objective. Following excitation at 458, 514, or 543 nm, cyan fluorescent protein (CFP) emission with a 475–525-nm band-pass barrier filter, yellow fluorescent protein (YFP) emission with a 530–600-nm band-pass barrier filter, or mCherry emission with a 650-nm long-pass barrier filter, respectively, was collected. The CD63–mCherry-positive vesicle of interest was selected for photobleaching of YFP. A protocol was then used which recorded pre- and post-bleaching images using 458-nm excitation at 10% laser power to limit photobleaching, with a bleaching of the selected area with 100% of the 514-nm laser power for 100 iterations (acceptor photobleaching). FRET was resolved as an increase in the CFP (donor) signal after photobleaching of YFP (acceptor). FRET efficiency (E) can be determined from the relative fluorescence intensity of the energy donor (CFP) before (I_{pre}) and after (I_{post}) photobleaching of the energy acceptor (YFP): $E = 1 - (I_{pre}/I_{post})$.

Analysis of F-actin formation on MVEs

The F-actin formation assay was performed using a SiR-actin kit (Spirochrome, Stein am Rhein, Switzerland) (31). HeLa cells expressing CD63–mCherry and FLAG–Rab5 (Q79L), or expressing CD63–mCherry and FLAG–Rab5 (Q79L) with Myc–Cdc42 (Q61L), Myc–Rac1 (Q61L), or FLAG–GRK2ct were incubated with 100 nM SiR–actin with vehicle or the indicated inhibitors for 24 h in culture conditions, followed by fixation with 4% paraformaldehyde in phosphate-buffered saline. The CD63–mCherry-positive vesicle of interest was subjected to F-actin formation analysis using a LSM 510 META with a ×63 oil plan-apochromat objective. Following excitation at 543 or 633 nm, mCherry emission with a 560–615-nm band-pass barrier filter and SiR–actin emission with a 650-nm long-pass barrier filter were collected, respectively. For all image acquisitions, the condition setting was fixed with an optimal value. The F-actin formation was quantified as the mean of SiR–actin fluorescence intensity on MVE using ImageJ software.

Analysis of cargo sorting into MVEs

HeLa cells plated on glass-bottomed 35-mm culture dishes were transiently expressed with CD63–GFP and Rab5 (Q79L)–DsRed, then cells were fixed with 4% paraformaldehyde in phosphate-buffered saline 3 days after transfection. Images were then obtained using a LSM 510 META with a ×63 oil plan-apochromat objective, optical zooms with ×6, and optical slice <0.9 μm. Following excitation at 488 or 543 nm, GFP emission with a 505–530-nm band-pass barrier filter and DsRed emission with a 560–615-nm band-pass barrier filter were collected, respectively. The amount of CD63–GFP in the endosomal lumen was quantified as fluorescence intensity in the lumen *versus* the limiting membrane of enlarged vesicle (diameter; >1 μm) using ImageJ software.

Quantification of cargo content per each exosome

Quantification of cargo content per each exosome was carried out essentially as reported previously (17). Briefly, purified exosomes from HeLa cell culture media were incubated with a mixture of 100 mg/liter of DOPE-biotin and 10 mg/liter of DiD for 15 min. A glass coverslip in a glass-bottomed 35-mm culture dish was incubated with a mixture of 0.1 g/liter of BSA/BSA-biotin. Excess protein was removed by gently flushing the surface with PBS and subsequently incubated for 10 min with 0.025 g/liter of streptavidin. After gently rinsing with PBS, DOPE–biotin- and DiD-labeled exosomes resuspended in equivolumes were added onto the surface-functionalized glass coverslip. The fluorescence of GFP and DiD were observed under a confocal laser scanning microscope (LSM 510 META).

Statistical analyses

Results are expressed as median on scatter-dot plots. Data were analyzed by Welch's *t* test using GraphPad Prism 6.0 (GraphPad Software, Inc., San Diego, CA). p values < 0.05 were considered significant.

Author contributions—T. K., T. O., and S.-i. N. conceived the project and designed the experiments; T. K., N. N. I. M., S. M. M. B., S. A. M., M. H., S. N., and D. Y. performed experiments; T. K., T. O., T. I., and S.-i. N. analyzed the data; S.-i. N. wrote the manuscript together with contributions from T. K., T. O., and T. I. All authors edited and approved the final manuscript.

Acknowledgment—We thank R. Kharbas for comments on the manuscript.

References

1. Théry, C., Ostrowski, M., and Segura, E. (2009) Membrane vesicles as conveyors of immune responses. *Nat. Rev. Immunol.* **9,** 581–593 CrossRef Medline
2. Peinado, H., Alečković, M., Lavotshkin, S., Matei, I., Costa-Silva, B., Moreno-Bueno, G., Hergueta-Redondo, M., Williams, C., García-Santos, G., Ghajar, C., Nitadori-Hoshino, A., Hoffman, C., Badal, K., Garcia, B. A., Callahan, M. K., *et al.* (2012) Melanoma exosomes educate bone marrow progenitor cells toward a pro-metastatic phenotype through MET. *Nat. Med.* **18,** 883–891 CrossRef Medline
3. Rajendran, L., Honsho, M., Zahn, T. R., Keller, P., Geiger, K. D., Verkade, P., and Simons, K. (2006) Alzheimer's disease beta-amyloid peptides are released in association with exosomes. *Proc. Natl. Acad. Sci. U.S.A.* **103,** 11172–11177 CrossRef Medline
4. Gruenberg, J., and Stenmark, H. (2004) The biogenesis of multivesicular endosomes. *Nat. Rev. Mol. Cell Biol.* **5,** 317–323 CrossRef Medline
5. Piper, R. C., and Katzmann, D. J. (2007) Biogenesis and function of multivesicular bodies. *Annu. Rev. Cell Dev. Biol.* **23,** 519–547 CrossRef Medline
6. Raiborg, C., Bache, K. G., Gillooly, D. J., Madshus, I. H., Stang, E., and Stenmark, H. (2002) Hrs sorts ubiquitinated proteins into clathrin-coated microdomains of early endosomes. *Nat. Cell Biol.* **4,** 394–398 CrossRef Medline
7. Hanson, P. I., and Cashikar, A. (2012) Multivesicular body morphogenesis. *Annu. Rev. Cell Dev. Biol.* **28,** 337–362 CrossRef Medline
8. Stuffers, S., Sem Wegner, C., Stenmark, H., and Brech, A. (2009) Multivesicular endosome biogenesis in the absence of ESCRTs. *Traffic* **10,** 925–937 CrossRef Medline
9. Wubbolts, R., Leckie, R. S., Veenhuizen, P. T., Schwarzmann, G., Möbius, W., Hoernschemeyer, J., Slot, J. W., Geuze, H. J., and Stoorvogel, W. (2003) Proteomic and biochemical analyses of human B cell-derived exosomes. Potential implications for their function and multivesicular body formation. *J. Biol. Chem.* **278,** 10963–10972 CrossRef Medline
10. Trajkovic, K., Hsu, C., Chiantia, S., Rajendran, L., Wenzel, D., Wieland, F., Schwille, P., Brügger, B., and Simons, M. (2008) Ceramide triggers budding of exosome vesicles into multivesicular endosomes. *Science* **319,** 1244–1247 CrossRef Medline
11. Perry, D. K., and Hannun, Y. A. (1998) The role of ceramide in cell signaling. *Biochim. Biophys. Acta* **1436,** 233–243 CrossRef Medline
12. Pyne, S., and Pyne, N. J. (2000) Sphingosine 1-phosphate signalling in mammalian cells. *Biochem. J.* **349,** 385–402 CrossRef Medline
13. Spiegel, S., and Milstien, S. (2002) Sphingosine 1-phosphate, a key cell signaling molecule. *J. Biol. Chem.* **277,** 25851–25854 CrossRef Medline
14. Le Stunff, H., Milstien, S., and Spiegel, S. (2004) Generation and metabolism of bioactive sphingosine-1-phosphate. *J. Cell. Biochem.* **92,** 882–899 CrossRef Medline
15. Pyne, S., Long, J. S., Ktistakis, N. T., and Pyne, N. J. (2005) Lipid phosphate phosphatases and lipid phosphate signalling. *Biochem. Soc. Trans.* **33,** 1370–1374 CrossRef Medline
16. Rosen, H., Gonzalez-Cabrera, P. J., Sanna, M. G., and Brown, S. (2009) Sphingosine 1-phosphate receptor signaling. *Annu. Rev. Biochem.* **78,** 743–768 CrossRef Medline
17. Kajimoto, T., Okada, T., Miya, S., Zhang, L., and Nakamura, S. (2013) Ongoing activation of sphingosine 1-phosphate receptors mediates maturation of exosomal multivesicular endosomes. *Nat. Commun.* **4,** 2712 Medline
18. Yoshizaki, H., Ohba, Y., Kurokawa, K., Itoh, R. E., Nakamura, T., Mochizuki, N., Nagashima, K., and Matsuda, M. (2003) Activity of Rho-family GTPases during cell division as visualized with FRET-based probes. *J. Cell Biol.* **162,** 223–232 CrossRef Medline
19. Bonacci, T. M., Mathews, J. L., Yuan, C., Lehmann, D. M., Malik, S., Wu, D., Font, J. L., Bidlack, J. M., and Smrcka, A. V. (2006) Differential targeting of Gβγ-subunit signaling with small molecules. *Science* **312,** 443–446 CrossRef Medline
20. Riven, I., Iwanir, S., and Reuveny, E. (2006) GIRK channel activation involves a local rearrangement of a preformed G protein channel complex. *Neuron* **51,** 561–573 CrossRef Medline
21. Koch, W. J., Hawes, B. E., Inglese, J., Luttrell, L. M., and Lefkowitz, R. J. (1994) Cellular expression of the carboxyl terminus of a G protein-coupled receptor kinase attenuates G βγ-mediated signaling. *J. Biol. Chem.* **269,** 6193–6197 Medline
22. Welch, H. C., Coadwell, W. J., Ellson, C. D., Ferguson, G. J., Andrews, S. R., Erdjument-Bromage, H., Tempst, P., Hawkins, P. T., and Stephens, L. R. (2002) P-Rex1, a PtdIns(3,4,5)P_3- and Gβγ-regulated guanine-nucleotide exchange factor for Rac. *Cell* **108,** 809–821 CrossRef Medline
23. Ueda, H., Nagae, R., Kozawa, M., Morishita, R., Kimura, S., Nagase, T., Ohara, O., Yoshida, S., and Asano, T. (2008) Heterotrimeric G protein βγ subunits stimulate FLJ00018, a guanine nucleotide exchange factor for Rac1 and Cdc42. *J. Biol. Chem.* **283,** 1946–1953 CrossRef Medline
24. Prehoda, K. E., Scott, J. A., Mullins, R. D., and Lim, W. A. (2000) Integration of multiple signals through cooperative regulation of the N-WASP-Arp2/3 complex. *Science* **290,** 801–806 CrossRef Medline
25. Rohatgi, R., Ho, H. Y., and Kirschner, M. W. (2000) Mechanism of N-WASP activation by CDC42 and phosphatidylinositol 4, 5-bisphosphate. *J. Cell Biol.* **150,** 1299–1310 CrossRef Medline
26. Miki, H., Yamaguchi, H., Suetsugu, S., and Takenawa, T. (2000) IRSp53 is an essential intermediate between Rac and WAVE in the regulation of membrane ruffling. *Nature* **408,** 732–735 CrossRef Medline
27. Eden, S., Rohatgi, R., Podtelejnikov, A. V., Mann, M., and Kirschner, M. W. (2002) Mechanism of regulation of WAVE1-induced actin nucleation by Rac1 and Nck. *Nature* **418,** 790–793 CrossRef Medline
28. Takenawa, T., and Suetsugu, S. (2007) The WASP-WAVE protein network: connecting the membrane to the cytoskeleton. *Nat. Rev. Mol. Cell Biol.* **8,** 37–48 CrossRef Medline
29. Ledezma-Sánchez, B. A., García-Regalado, A., Guzmán-Hernández, M. L., and Vázquez-Prado, J. (2010) Sphingosine-1-phosphate receptor $S1P_1$ is regulated by direct interactions with P-Rex1, a Rac guanine nucleotide exchange factor. *Biochem. Biophys. Res. Commun.* **391,** 1647–1652 CrossRef Medline
30. Naito, Y., and Ui-Tei, K. (2013) Designing functional siRNA with reduced off-target effects. *Methods Mol. Biol.* **942,** 57–68
31. Lukinavičius, G., Reymond, L., D'Este, E., Masharina, A., Göttfert, F., Ta, H., Güther, A., Fournier, M., Rizzo, S., Waldmann, H., Blaukopf, C., Sommer, C., Gerlich, D. W., Arndt, H. D., Hell, S. W., and Johnsson, K. (2014) Fluorogenic probes for live-cell imaging of the cytoskeleton. *Nat. Methods* **11,** 731–733 CrossRef Medline